Letter

Quantum interference tuning of spin-orbit coupling in twisted van der Waals trilayers

Csaba G. Péterfalvi,[1,*] Alessandro David,[2] Péter Rakyta,[3,4] Guido Burkard,[1,†] and Andor Kormányos[3,‡]

[1]*Department of Physics, University of Konstanz, D-78464 Konstanz, Germany*

[2]*Peter Grünberg Institute - Quantum Control (PGI-8), Forschungszentrum Jülich GmbH, Jülich, Germany*

[3]*Department of Physics of Complex Systems, Eötvös Loránd University, Budapest, Hungary*

[4]*Quantum Information National Laboratory, Hungary*

(Received 4 November 2021; revised 2 March 2022; accepted 9 March 2022; published 31 May 2022)

We show that in van der Waals stacks of twisted hexagonal layers the proximity induced Rashba spin-orbit coupling can be affected by quantum interference. We calculate the quantum phase responsible for this effect in graphene–transition metal dichalcogenide bilayers as a function of interlayer twist angle. We show how this quantum phase affects the spin polarization of the graphene bands and discuss its potential effect on spin-to-charge conversion measurements. In twisted trilayers symmetries can be broken as well as restored for certain twist angles. This can be used to deduce the effects of induced spin-orbit coupling on spin-lifetime anisotropy and magnetoconductance measurements.

DOI: 10.1103/PhysRevResearch.4.L022049

Multilayer stacks of two-dimensional (2D) materials, commonly referred to as van der Waals (vdW) heterostructures, have become an important platform for exploring a wide range of exciting phenomena, because they offer electronic tunability and a large parameter space. Initially, bilayer structures served as a platform to study, e.g., the effects of a moire potential in graphene/hBN [1–4], the induced spin-orbit coupling (SOC) in graphene/transition metal dichalcogenide (TMDC) heterostructures [5–7], or strong electronic correlations in magic-angle twisted bilayer graphene (MATG) [8,9]. A natural next step is to add another layer, which introduces a second twist angle and/or a further layer of different properties and this can enhance the parameter space to tune the properties of the system in several ways. An exciting opportunity is to use MATG and induce SOC into the flat bands by adding a TMDC layer to the stack [10,11]. Further examples include the recent proposal of an engineered topological phase in WSe_2/bilayer graphene (BLG)/WSe_2 system [12], the external gate tunability of SOC through changing layer polarization in TMDC/BLG structures [13–16], and imprinting double moiré potential on graphene [17–19]. More generally, vdW multilayers can serve as a quantum simulator platform for strongly correlated physics and topological materials [20].

The proximity induced SOC plays a pivotal role in many of the above proposals. A number of recent experimental works based on weak antilocalization (WAL) [5–7,21–25], spin-lifetime anisotropy measurements [26–29], spin-Hall [30–33], and Rashba-Edelstein effect [32,34–36] proved that SOC is strongly enhanced in graphene/TMDC heterostructures, which also motivated theoretical work to understand these measurements [5,37–44]. Recently, Refs. [45–48] have also discussed the interlayer twist angle dependence of the induced SOC in graphene/TMDC. In particular, it has been noted [46,47] that the most general form of the induced Rashba-SOC in twisted graphene/TMDC heterostructures that obeys time reversal $\mathcal{T}$ and threefold rotation C_3 symmetries can be written as

$$H_R = \frac{\lambda_R}{2} e^{i\frac{s_z}{2}\vartheta_R}(\tau_z\sigma_x s_y - \sigma_y s_x)e^{-i\frac{s_z}{2}\vartheta_R}, \tag{1}$$

where $s_{x,y,z}$ ($\sigma_{x,y,z}$) are Pauli matrices acting in the spin (sublattice) space, and τ_z is a Pauli matrix acting on the valley degree of freedom of graphene. Both ϑ_R and λ_R are functions of the interlayer twist angle θ, which we do not show explicitly in order to ease the notations. H_R differs from the usual Rashba SOC term [49–51] $H_R = \frac{\lambda_R}{2}(\tau_z\sigma_x s_y - \sigma_y s_x)$ by a rotation of angle ϑ_R in spin-space. The terms containing ϑ_R appear because for a general interlayer twist angle the symmetry of the heterostructure is lowered from C_{3v} to C_3. Thus, Eq. (1) is valid not only for graphene/TMDC heterostructures, but for a wide range of twisted heterostructures consisting of hexagonal layers, such as heterostructures of graphene with semiconductor [52,53], ferromagnetic [54], and topological insulator [55,56] structures. This general nature of the effect is one of the main motivations for our work. However, the physical significance of this spin-space rotation was not previously appreciated and the relation of ϑ_R to the interlayer twist angle θ has not been discussed. As we will show, using graphene/TMDC twisted bilayers as an example, ϑ_R can take finite values and it leads to quantum interference affecting the induced Rashba type SOC in twisted trilayers. While it has been known that λ_R is tunable, e.g., by pressure [57] in

*csaba.peterfalvi@uni-konstanz.de
†guido.burkard@uni-konstanz.de
‡andor.kormanyos@ttk.elte.hu

Published by the American Physical Society under the terms of the Creative Commons Attribution 4.0 International license. Further distribution of this work must maintain attribution to the author(s) and the published article's title, journal citation, and DOI.

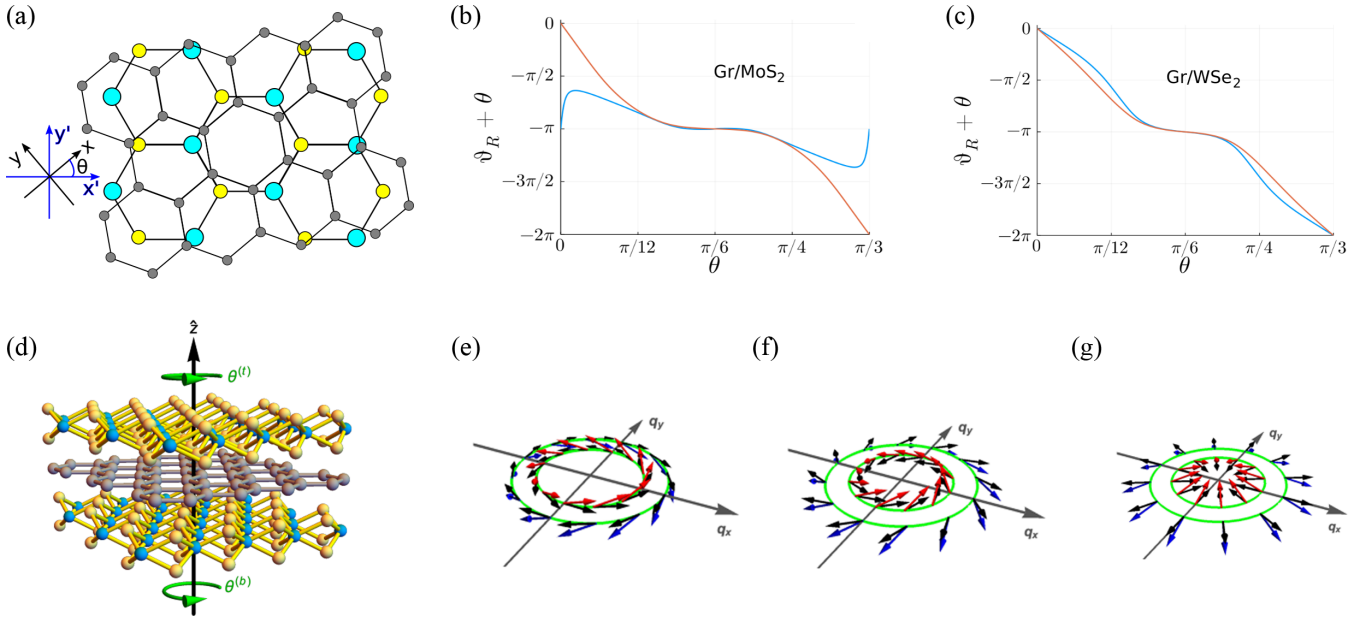

FIG. 1. (a) Schematics of a twisted graphene/TMDC bilayer with twist angle θ. (b) and (c) $\vartheta_R + \theta$ as a function of θ for MoS_2 and WSe_2. Blue (red) curves were calculated using DFT (ARPES measurements) parameters, see main text for details. (d) Schematics of a twisted TMDC/graphene/TMDC trilayer. The spin-orbit field $\mathbf{s}(\mathbf{q})$ for (e) $\theta = 0$, (f) $\theta = 7^\circ$, and (g) for $\theta = 15^\circ$, using the ϑ_R vs θ dependence shown in Fig. 1(c), calculated for graphene/WSe_2. The green circles indicate the Fermi surfaces for the two spin subbands. $\mathbf{s}(\mathbf{q})$ lies in the plane if only Rashba SOC is induced in graphene (black arrows), whereas it acquires a nonzero $\langle \hat{s}_z \rangle$ component if the valley Zeeman type SOC is finite as well (blue and red).

proximity structures, to our knowledge the possibility that quantum interference can affect its value has not been considered before.

Twisted bilayers. In order to obtain the angle ϑ_R, we use the methodology recently developed to calculate the coupling strength λ_R for graphene/TMDC bilayers [47]. ϑ_R is a quantum phase which depends on the interlayer tunneling between the Bloch states of graphene and the TMDC layer and on certain off-diagonal matrix elements of the intrinsic SOC of the TMDC, for details we refer to Ref. [58]. One finds that λ_R and ϑ_R are the absolute value and the phase of the complex Rashba coefficient $\bar{\lambda}_R = \lambda_R e^{i\vartheta_R}$, which is given by the sum of the contributions from pairs of even (e) and odd (o) bands of the TMDC: $\bar{\lambda}_R = \sum_q \lambda_{R,(e,o)_q} e^{i\vartheta_{(e,o)q}} = \sum_q \lambda_{R,q} e^{i\vartheta_q}$. Here $\lambda_{R,q}$ and ϑ_q are the magnitude and the phase of the contributions of the pairs of bands. In the calculations of $\lambda_{R,q}$ and ϑ_q we have used the tight-binding model of Ref. [59]. For the initial steps of the calculations it is convenient to assume that the graphene layer is rotated with respect to the TMDC layer [47]. In the final steps we change the representation of the Hamiltonian from the coordinate system fixed to the TMDC layer to the system fixed to the graphene layer with a transformation $e^{-i\tau_z \frac{\sigma_z}{2}\theta} H_R e^{i\tau_z \frac{\sigma_z}{2}\theta}$, see Fig. 1(a). From the explicit form of the transformed Rashba Hamiltonian one finds that the nonzero matrix elements are $\propto \lambda_R e^{\pm i(\vartheta_R + \theta)}$, i.e., the sum of the geometric angle θ and the quantum phase ϑ_R plays an important role.

Regarding our numerical calculations, the first ingredient is the tight-binding (TB) Hamiltonian of Ref. [59] for TMDCs. This TB model itself is derived from density functional theory (DFT) calculations and we use it, among others, to calculate matrix elements of the spin-orbit coupling Hamiltonian and the interlayer tunneling amplitude. The results also depend on (i) the position of the Dirac point of graphene within the band gap E_g of the TMDC, and (ii) on the value of E_g. Numerical DFT calculations are known to often underestimate E_g and they seem to give [37] different results from experiments [60,61] for the energy alignment of graphene's Dirac point with the TMDC bands. We performed our calculations for two parameter sets to assess how sensitive are the results on the choice of these material parameters. Since Ref. [59] does not provide information on the band alignment of graphene and the TMDC layer, we use the DFT calculations of Ref. [37] for this purpose. The second parameter set for E_g and the band alignment is extracted from ARPES measurements [60,61]. Since the coupling between the layers is weak at the Dirac point of graphene, the band alignment should mainly depend on the work function difference between the two materials. Therefore, we assume that it does not depend on the interlayer twist angle. This is in agreement with the recent computational work of Ref. [62].

The results for the $\vartheta_R + \theta$ vs θ dependence for two selected TMDCs, MoS_2 and WSe_2, are shown in Figs. 1(b) and 1(c), respectively. In the case of MoS_2, using the DFT parameter set, one can see that $\vartheta_R + \theta$ remains in a limited range around π as θ varies from 0 to $\pi/3$ [Fig. 1(b)]. However, if parameters extracted from ARPES measurements [60] are used, then $\vartheta_R + \theta$ covers the entire range $[0, 2\pi]$. For WSe_2 one finds that $\vartheta_R + \theta$ covers all of $[0, 2\pi]$ [Fig. 1(c)] and the results obtained from the two parameter sets qualitatively agree. The difference between the results for the two materials can be mainly traced back to the different energy alignment of the Dirac point in the TMDC band gap. One can also note in Figs. 1(b) and 1(c) that for $\theta = l\pi/6$, $l = 0, 1, \ldots$ one

finds $\vartheta_R + \theta = n\pi$, where n is an integer. We give a detailed discussion of how this result for $\vartheta_R + \theta$ follows from our theoretical method in Ref. [58], but already note at this point that for $\theta = l\pi/6$ the vertical mirror planes of the graphene and the TMDC lattice line up and the system, as a whole, has C_{3v} symmetry. In this case the Hamiltonian of the induced Rashba SOC reads $H_R = (-1)^{n+1}\frac{\lambda_R(\theta)}{2}(\tau_z\sigma_x s_y - \sigma_y s_x)$, hence H_R simplifies to the form used previously in the literature [37,49]. We find that n can be, in general, both odd and even [see Figs. 1(b) and 1(c)], which means that $\lambda_R(\theta)$ can acquire a negative sign as θ is changed. Interestingly, when $\vartheta_R + \theta \neq n\pi$, the spin-orbit field $\mathbf{s}(\mathbf{q}) = (\langle\hat{s}_x\rangle, \langle\hat{s}_y\rangle, \langle\hat{s}_z\rangle)^T$ is not tangential to the Fermi surface as in the case of usual Rashba SOC [cf. Figs. 1(e)–1(g)]. Instead, one can show that the in-plane component $(\langle\hat{s}_x\rangle, \langle\hat{s}_y\rangle)^T$ is rotated by an angle $\vartheta_R + \theta$ with respect to the tangential direction. As we will discuss, this might have consequences on the interpretation of experimental results.

Twisted TMDC/graphene/TMDC trilayers. Adding another TMDC layer, as shown in Fig. 1(d), introduces a second interlayer twist angle and the two twist angles $\theta^{(b)}$ and $\theta^{(t)}$ for the bottom and top TMDC layers allow an even broader control of the induced SOC in graphene.

Since the layers are only weakly coupled, the effective graphene Hamiltonian is $H_{\rm orb} + H^{(t)}_{\rm soc} + H^{(b)}_{\rm soc}$, where $H^{(b)}_{\rm soc} = H^{(b)}_{\rm vZ} + H^{(b)}_R$ and $H^{(t)}_{\rm soc} = H^{(t)}_{\rm vZ} - H^{(t)}_R$. Here $H_{\rm vZ} = \lambda_{\rm vZ}\tau_z s_z$ is the Hamiltonian of the induced valley Zeeman SOC in the graphene layer. Note that the contributions $H^{(b)}_R$ and $H^{(t)}_R$ have a different sign. As a simple physical explanation, consider the case when the two TMDC layers are perfectly aligned, e.g., $\theta^{(b)} = \theta^{(t)}$. Then the graphene layer is a horizontal mirror plane of the whole stack, which dictates that the Rashba SOC must vanish. (A more microscopic argument is given in Ref. [58].) One can define the complex Rashba coefficient for the trilayer system (tls) by

$$\bar{\lambda}^{(\rm tls)}_R = \lambda^{(b)}_R e^{i(\vartheta^{(b)}_R + \theta^{(b)})} - \lambda^{(t)}_R e^{i(\vartheta^{(t)}_R + \theta^{(t)})}, \tag{2}$$

and its magnitude $\lambda^{(\rm tls)}_R = |\bar{\lambda}^{(\rm tls)}_R|$ and phase $\vartheta^{(\rm tls)} = {\rm Arg}[\bar{\lambda}^{(\rm tls)}_R]$. In terms of these quantities the induced Rashba type SOC can be written as $H^{(\rm tls)}_R = \frac{\lambda^{(\rm tls)}_R}{2} e^{i\frac{s_z}{2}\vartheta^{(\rm tls)}}(\tau_z\sigma_x s_y - \sigma_y s_x)e^{-i\frac{s_z}{2}\vartheta^{(\rm tls)}}$. The importance of the phase $e^{i(\vartheta_R+\theta)}$ discussed for bilayers becomes now more clear: it follows from Eq. (2) that the strength $\lambda^{(\rm tls)}_R$ of the induced Rashba SOC in trilayer stacks can be affected by quantum interference effects if $\vartheta^{(b)}_R + \theta^{(b)}$ and/or $\vartheta^{(t)}_R + \theta^{(t)}$ are nonzero. This can be interpreted as an interference of the virtual hopping processes to the two TMDC layers that give rise to the induced Rashba SOC. Calculations for the twist angle dependence of λ_R have already been performed in Refs. [46,47], therefore we do not show these results here, see Ref. [58] for further details. The results of our numerical calculations for $H^{(\rm tls)}_R$ are summarized in Figs. 2(a)–2(d). First, symmetries that are broken in bilayers can be restored in trilayers for certain $\theta^{(b)}$ and $\theta^{(t)}$ angles. If $|\theta^{(b)} - \theta^{(t)}| = l\pi/3$, where l is an odd integer, the trilayer stack is inversion symmetric. On the other hand, for an even l the stack has a horizontal mirror plane. Therefore the induced Rashba SOC must vanish for any integer l, as it can be seen in Figs. 2(a) and 2(b). For WSe_2 encapsulation [Fig. 2(a)] the

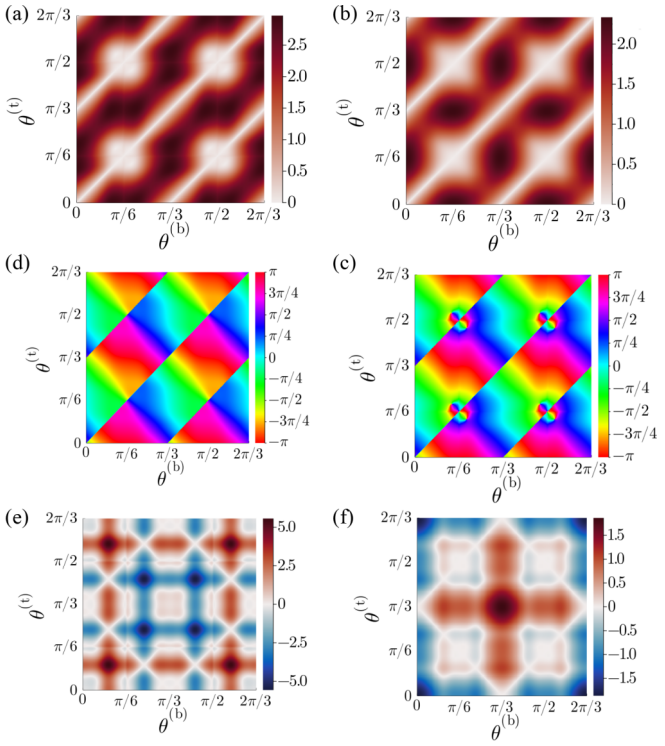

FIG. 2. (a) and (b) $\lambda^{(\rm tls)}_R$ for MoS_2 and WSe_2 two-sided encapsulation. (c) and (d) The angle $\vartheta^{(\rm tls)}$ for MoS_2 and WSe_2 two-sided encapsulation. (e) and (f) $\lambda^{(\rm tls)}_{\rm vZ}$ for MoS_2 and WSe_2 two-sided encapsulation. We used parameters from DFT band structure calculations, see [63].

maximum of $\lambda^{(\rm tls)}_R$ is found for $|\theta^{(b)} - \theta^{(t)}| = (2l+1)\pi/6$. The maximum value of $\lambda^{(\rm tls)}_R$ is around 70% larger than in the graphene/WSe_2 case. Thus, double-sided encapsulation can significantly enhance the induced Rashba SOC. Surprisingly, when using MoS_2 for double encapsulation [Fig. 2(b)], we find that $\lambda^{(\rm tls)}_R$ basically cannot be enhanced above the value obtained for one sided proximity effect. This can be understood by considering the explicit dependence of $\lambda^{(t,b)}_R$ and $\vartheta^{(t,b)}_R$ on $\theta^{(t,b)}$, see Ref. [58] for details. The origin of the extended regions where $\lambda^{(\rm tls)}_R$ is very small is due to the fact that for those twist angles λ_R and ϑ_R change slowly in both layers and therefore they approximately cancel in Eq. (2). In Figs. 2(c) and 2(d) we show the phase $\vartheta^{(\rm tls)}$ of Eq. (2), which determines the winding of the SOC field $\mathbf{s}(\mathbf{q})$ in the case of double encapsulation. The apparent diagonal lines correspond to $\lambda^{(\rm tls)}_R = 0$ where $\vartheta^{(\rm tls)}$ is not defined.

For completeness, we also discuss the twist angle dependence of the induced valley Zeeman SOC in TMDC/graphene/TMDC trilayers, see Figs. 2(e) and 2(f). The strength of the valley Zeeman type SOC is simply given by $\lambda^{(\rm tls)}_{\rm vZ} = \lambda^{(b)}_{\rm vZ}(\theta^{(b)}) + \lambda^{(t)}_{\rm vZ}(\theta^{(t)})$. If the two TMDC layers are (nearly) aligned, they can *double* the strength of the induced valley Zeeman SOC. When the whole stack has inversion symmetry, the effect of the two layers cancel and $\lambda^{(\rm tls)}_{\rm vZ} = 0$. The valley Zeeman SOC also vanishes along the lines $\theta^{(b)} + \theta^{(t)} = \pi/3, \pi$, this is a combined effect of time reversal and threefold rotation symmetry of the TMDC layers. We also

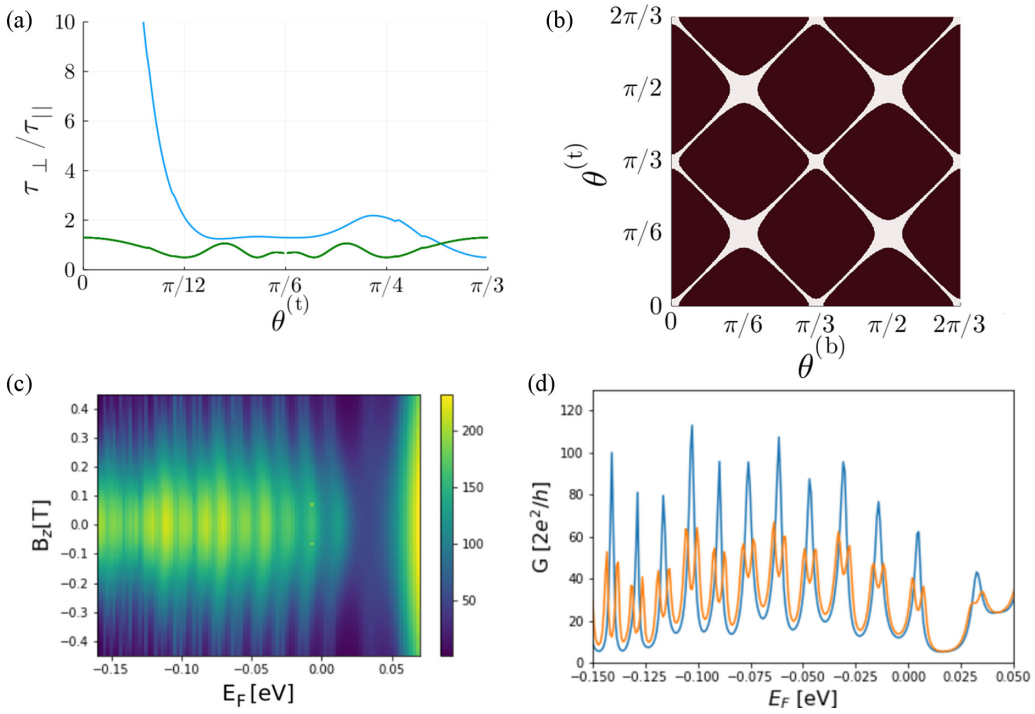

FIG. 3. (a) Calculated spin lifetime anisotropy in a TMDC/graphene/TMDC heterostructure as a function of $\theta^{(t)}$ for $\theta^{(b)} = 0^\circ$ (blue) and $\theta^{(b)} = 30^\circ$ (green). (b) White color indicates the regions in the $(\theta^{(t)}, \theta^{(b)})$ space where the REE is expected to vanish for a WSe_2/graphene/WSe_2 trilayer. In the calculations for (a) and (b) we used DFT parameters [63]. (c) Conductance G (in units of $2e^2/h$) through an *npn* junction as a function of magnetic field B_z and Fermi energy E_F for $\lambda_{vZ} = 2.6$ meV. (d) Cross section of (c) at fixed $B_z = 0.436$ T. $\lambda_{vZ} = 0$ meV (blue) and $\lambda_{vZ} = 2.6$ meV (orange).

note that $\lambda_{vZ}^{(tls)}$ depends sensitively on what kind of TMDC is used in the stacks. The difference between the effects of WSe_2 [Fig. 2(e)] and MoS_2 [Fig. 2(f)] is mainly due to the different alignment of graphene's Dirac point with the TMDC bands. The calculations shown in Fig. 2, together with Eq. (2), are the main results of this work.

In the preceding discussions of graphene/TMDC and TMDC/graphene/TMDC heterostructures we have neglected a possible lateral shift of the graphene layer with respect to the TMDCs and moiré effects. Regarding the lateral shift, it does not affect our results [58]. Considering the moiré effects, in graphene/TMDC bilayers they are present only at energy scales larger than 2 eV [58,60], i.e., they are negligible for energies close to the Dirac point of graphene. The situation might be different in TMDC/graphene/TMDC trilayers. Based on previous work of Refs. [64,65] on hBN/graphene/hBN trilayers, one may expect that supermoiré effects may become important when the TMDC layers are nearly aligned: $0 < |\theta^{(t)} - \theta^{(b)}| \lesssim 1^\circ$ (see Ref. [58] for further details). The discussion of supermoiré is beyond the scope of the present work.

Experimental predictions. Several recent works [26,28,29] measured an anisotropy of the out-of-plane $\tau_\perp$ and in-plane $\tau_\parallel$ spin lifetimes in graphene/TMDC heterostructures which can be interpreted as direct proof of induced SOC in graphene. Namely, according to the theoretical calculations of Ref. [39], if there is a strong intervalley scattering in graphene, then the ratio of the spin lifetimes is given by $\tau_\perp/\tau_\parallel = (\lambda_{vZ}/\lambda_R)^2(\tau_{iv}/\tau_p) + 1/2$, where τ_{iv} (τ_p) is the intervalley (momentum) scattering time. (For ultraclean samples with SOC comparable to or larger than the disorder-induced quasiparticle broadening, a qualitatively different spin relaxation anisotropy is derived in Ref. [66].) Let us consider a WSe_2/graphene/WSe_2 heterostructure and assume that $\theta^{(b)}$ is kept fixed while $\theta^{(t)}$ is changed. Note that the ratio λ_{vZ}/λ_R can be tuned in a wider range in trilayer structures than in bilayers. For example, λ_R is never zero for graphene/TMDC, whereas one can choose $\theta^{(b)}$ and $\theta^{(t)}$ such that $\lambda_{vZ}^{(tls)} \neq 0$ and $\lambda_R^{(tls)} = 0$, see Figs. 2(a) and 2(e). Using $\tau_{iv}/\tau_p \approx 5$ as in Ref. [39], we plot $\tau_\perp/\tau_\parallel$ as a function of $\theta^{(t)}$ for $\theta^{(b)} = 0^\circ$ and $\theta^{(b)} = 30^\circ$ in Fig. 3(a). When $\theta^{(b)} = 0$ and $1^\circ < \theta^{(t)} \lesssim 15^\circ$ then $\lambda_R^{(tls)}$ becomes small but $\lambda_{vZ}^{(tls)}$ is finite, therefore $\tau_\perp/\tau_\parallel$ strongly increases as a function of $\theta^{(t)}$. This enhancement happens before supermoiré effects might become important for $\theta^{(t)} \lesssim 1^\circ$. In contrast, if $\theta^{(b)} = 30^\circ$, then $\tau_\perp/\tau_\parallel$ remains finite for all $\theta^{(t)}$ angles. This dramatic difference in the $\theta^{(t)}$ dependence of $\tau_\perp/\tau_\parallel$ is clearly a consequence of the wider tunability of $\lambda_{vZ}^{(tls)}/\lambda_R^{(tls)}$ in trilayers.

One can expect that charge-to-spin conversion measurements should also be affected by the interlayer twist. Let us consider a graphene/TMDC bilayer and for simplicity assume that (i) $\lambda_{vZ} \ll \lambda_R$ and (ii) a DC electric field is applied along the $\hat{x}$ direction. In steady state the $\hat{y}$ component of the spin density is given by $\langle S_y \rangle = \frac{1}{2}\int \frac{d^2\mathbf{q}}{4\pi} s_y(\mathbf{q})\delta f_\mathbf{q}$ where $\delta f_\mathbf{q}$ is the deviation of the quasiparticle distribution with respect to equilibrium. Using the semiclassical argument given in Ref. [41], for Fermi energies close to the Dirac point E_D such that $|E_F - E_D| < \lambda_R(\theta)$, i.e., when there is a single Fermi sur-

face, one finds that $\langle S_y \rangle \propto \cos(\vartheta_R + \theta)$. This suggests that the Rashba-Edelstein effect (REE) may vanish [when $\vartheta_R + \theta = (2l+1)\pi/2$] even though $\lambda_R(\theta)$ is not required to be zero by symmetry for any θ. $\langle S_y \rangle$ can also change sign as a function of the interlayer twist angle, because $\vartheta_R + \theta \in [0, 2\pi]$, see Figs. 1(b) and 1(c). Regarding the more realistic situation when there are two spin-polarized Fermi surfaces in graphene for $|E_F - E_D| > \lambda_R$, looking at Fig. 1(g) one can understand that $\langle S_y \rangle$ can be zero as a function of twist angle in this case as well. Furthermore, in twisted TMDC/graphene/TMDC trilayers, the REE can vanish either because $\lambda_R^{(\mathrm{tls})} = 0$ or because $\vartheta^{(\mathrm{tls})} = (2l+1)\pi/2$, which can be expressed compactly as $\mathrm{Re}(\bar{\lambda}_R^{(\mathrm{tls})}) = 0$. As an example, the region where this condition is fulfilled in the $(\theta^{(t)}, \theta^{(b)})$ space for WSe_2/graphene/WSe_2 trilayers is shown in Fig. 3(b).

While the spin-lifetime anisotropy measurements require diffusive samples, in Figs. 3(c) and 3(d) we show an example of how strong SOC can affect ballistic transport properties. Highly transparent *np* and *npn* junctions in graphene have recently been realized in several experiments [67–71] and Fabry-Perrot type interference measurements [71]. Assume now that a TMDC/graphene/TMDC trilayer is tuned with interlayer twist angles such that the Rashba SOC is switched off and simultaneously the valley Zeeman SOC enhanced. We calculate the conductance [58] through a smooth graphene *npn* junction [72] as a function of out-of-plane magnetic field B_z and Fermi energy E_F for $\lambda_{vZ} = 2.6$ meV, see Fig. 3(c). One can observe that for $|B_z| > 0.3$ T the high-conductance ridges are split. This is apparent in Fig. 3(d), where we compare the cases when $\lambda_{vZ} = 0$ (blue) and $\lambda_{vZ} = 2.6$ meV (orange) for a fixed magnetic field $B_z = 0.436$ T. Our calculations also indicate that the Rashba type SOC does not have a similar effect on the conductance ridges (not shown). An additional experimental probe of the twist angle dependent SOC may be the measurement of the reflection of electrons at a planar junction, which is briefly discussed in Ref. [58].

Summary. We found that the induced Rashba type SOC in twisted hexagonal bilayers can be parametrized by the strength λ_R and a spin-rotation angle ϑ_R. This latter can lead to interference effects for λ_R in trilayer heterostructures. We also calculated the valley Zeeman SOC in twisted TMDC/graphene/TMDC trilayers. Finally, we discussed how the interlayer twist angle dependence of the induced SOC can be deduced from spin-lifetime anisotropy, charge-to-spin conversion, and magnetrotransport measurements.

In this work we have neglected possible lattice relaxation in vdW heterostructures [73]. An important future direction would be to study its effect on the results presented here.

Note added. During the preparation of this manuscript we have become aware of Ref. [62], where the authors discuss the twist angle dependence of the induced SOC in graphene/TMDC structures using DFT calculations.

Acknowledgments. We acknowledge helpful conversations with Péter Makk and Jaroslav Fabian. This research was supported by the Ministry of Innovation and Technology and the National Research, Development and Innovation Office (NKFIH) within the Quantum Information National Laboratory of Hungary. P.R. and A.K. were also supported by the ELTE Institutional Excellence Program (TKP2020-IKA-05), and the Hungarian Scientific Research Fund (OTKA) Grants No. K134437 and No. NN127903 (Topograph FlagERA project). A.K. acknowledges support from the Hungarian Academy of Sciences through the Bolyai János Stipendium (BO/00603/20/11) as well.

[1] M. Yankowitz, J. Xue, D. Cormode, J. D. Sanchez-Yamagishi, K. Watanabe, T. Taniguchi, P. Jarillo-Herrero, P. Jacquod, and B. J. LeRoy, Emergence of superlattice Dirac points in graphene on hexagonal boron nitride, Nat. Phys. **8**, 382 (2012).

[2] L. A. Ponomarenko, R. V. Gorbachev, G. L. Yu, D. C. Elias, R. Jalil, A. A. Patel, A. Mishchenko, A. S. Mayorov, C. R. Woods, J. R. Wallbank, M. Mucha-Kruczynski, B. A. Piot, M. Potemski, I. V. Grigorieva, K. S. Novoselov, F. Guinea, V. I. Fal'ko, and A. K. Geim, Cloning of Dirac fermions in graphene superlattices, Nature (London) **497**, 594 (2013).

[3] B. Hunt, J. D. Sanchez-Yamagishi, A. F. Young, M. Yankowitz, B. J. LeRoy, K. Watanabe, T. Taniguchi, P. Moon, M. Koshino, P. Jarillo-Herrero, and R. C. Ashoori, Massive Dirac fermions and Hofstadter butterfly in a van der Waals heterostructure, Science **340**, 1427 (2013).

[4] R. Ribeiro-Palau, C. Zhang, K. Watanabe, T. Taniguchi, J. Hone, and C. R. Dean, Twistable electronics with dynamically rotatable heterostructures, Science **361**, 690 (2018).

[5] Z. Wang, D.-K. Ki, H. Chen, H. Berger, A. H. MacDonald, and A. F. Morpurgo, Strong interface-induced spin-orbit interaction in graphene on WS_2, Nat. Commun. **6**, 8339 (2015).

[6] Z. Wang, D.-K. Ki, J. Y. Khoo, D. Mauro, H. Berger, L. S. Levitov, and A. F. Morpurgo, Origin and Magnitude of 'Designer' Spin-Orbit Interaction in Graphene on Semiconducting Transition Metal Dichalcogenides, Phys. Rev. X **6**, 041020 (2016).

[7] B. Yang, M.-F. Tu, J. Kim, Y. Wu, H. Wang, J. Alicea, R. Wu, M. Bockrath, and J. Shi, Tunable spin-orbit coupling and symmetry-protected edge states in graphene/WS_2, 2D Mater. **3**, 031012 (2016).

[8] R. Bistritzer and A. H. MacDonald, Moiré bands in twisted double-layer graphene, Proc. Natl. Acad. Sci. USA **108**, 12233 (2011).

[9] Y. Cao, V. Fatemi, S. Fang, K. Watanabe, T. Taniguchi, E. Kaxiras, and P. Jarillo-Herrero, Unconventional superconductivity in magic-angle graphene superlattices, Nature (London) **556**, 43 (2018).

[10] H. S. Arora, R. Polski, Y. Zhang, A. Thomson, Y. Choi, H. Kim, Z. Lin, I. Z. Wilson, X. Xu, J.-H. Chu, K. Watanabe, T. Taniguchi, J. Alicea, and S. Nadj-Perge, Superconductivity in metallic twisted bilayer graphene stabilized by WSe_2, Nature (London) **583**, 379 (2020).

[11] J.-X. Lin, Y.-H. Zhang, E. Morissette, Z. Wang, S. Liu, D. Rhodes, K. Watanabe, T. Taniguchi, J. Hone, and J. I. A. Li, Spin-orbit-driven ferromagnetism at half moiré filling in magic-angle twisted bilayer graphene, Science **375**, 437 (2022).

[12] J. O. Island, X. Cui, C. Lewandowski, J. Y. Khoo, E. M. Spanton, H. Zhou, D. Rhodes, J. C. Hone, T. Taniguchi, K. Watanabe, L. S. Levitov, M. P. Zaletel, and A. F. Young, Spin–orbit-driven band inversion in bilayer graphene by the van der Waals proximity effect, Nature (London) **571**, 85 (2019).

[13] J. Y. Khoo, A. F. Morpurgo, and L. Levitov, On-demand spin-orbit interaction from which-layer tunability in bilayer graphene, Nano Lett. **17**, 7003 (2017).

[14] M. Gmitra and J. Fabian, Proximity Effects in Bilayer Graphene on Monolayer WSe_2: Field-Effect Spin Valley Locking, Spin-Orbit Valve, and Spin Transistor, Phys. Rev. Lett. **119**, 146401 (2017).

[15] D. Wang, S. Che, G. Cao, R. Lyu, K. Watanabe, T. Taniguchi, C. N. Lau, and M. Bockrath, Quantum Hall effect measurement of spin-orbit coupling strengths in ultraclean bilayer graphene/WSe_2 heterostructures, Nano Lett. **19**, 7028 (2019).

[16] P. Tiwari, S. K. Srivastav, and A. Bid, Electric-Field-Tunable Valley Zeeman Effect in Bilayer Graphene Heterostructures: Realization of the Spin-Orbit Valve Effect, Phys. Rev. Lett. **126**, 096801 (2021).

[17] Z. Wang, Y. B. Wang, J. Yin, E. Tóvári, Y. Yang, L. Lin, M. Holwill, J. Birkbeck, D. J. Perello, S. Xu, J. Zultak, R. V. Gorbachev, A.V. Kretinin, T. Taniguchi, K. Watanabe, S. V. Morozov, M. Andjelković, S.P. Milovanović, L. Covaci, F. M. Peeters *et al.*, Composite super-moiré lattices in double-aligned graphene heterostructures, Sci. Adv. **5**, eaay8897 (2019).

[18] Z. Zhu, P. Cazeaux, M. Luskin, and E. Kaxiras, Modeling mechanical relaxation in incommensurate trilayer van der Waals heterostructures, Phys. Rev. B **101**, 224107 (2020).

[19] L. Wang, S. Zihlmann, M.-H. Liu, P. Makk, K. Watanabe, T. Taniguchi, A. Baumgartner, and C. Schönenberger, New generation of moiré superlattices in doubly aligned hBN/graphene/hBN heterostructures, Nano Lett. **19**, 2371 (2019).

[20] D. M. Kennes, M. Claassen, L. Xian, A. Georges, A. J. Millis, J. Hone, C. R. Dean, D. N. Basov, A. N. Pasupathy, and A. Rubio, Moiré heterostructures as a condensed-matter quantum simulator, Nat. Phys. **17**, 155 (2021).

[21] B. Yang, M. Lohmann, D. Barroso, I. Liao, Z. Lin, Y. Liu, L. Bartels, K. Watanabe, T. Taniguchi, and J. Shi, Strong electron-hole symmetric Rashba spin-orbit coupling in graphene/monolayer transition metal dichalcogenide heterostructures, Phys. Rev. B **96**, 041409(R) (2017).

[22] T. Völkl, T. Rockinger, M. Drienovsky, K. Watanabe, T. Taniguchi, D. Weiss, and J. Eroms, Magnetotransport in heterostructures of transition metal dichalcogenides and graphene, Phys. Rev. B **96**, 125405 (2017).

[23] S. Zihlmann, A. W. Cummings, J. H. Garcia, M. Kedves, K. Watanabe, T. Taniguchi, C. Schönenberger, and P. Makk, Large spin relaxation anisotropy and valley-Zeeman spin-orbit coupling in WSe_2/graphene/hBN heterostructures, Phys. Rev. B **97**, 075434 (2018).

[24] T. Wakamura, F. Reale, P. Palczynski, S. Guéron, C. Mattevi, and H. Bouchiat, Strong Anisotropic Spin-Orbit Interaction Induced in Graphene by Monolayer WS_2, Phys. Rev. Lett. **120**, 106802 (2018).

[25] T. Wakamura, F. Reale, P. Palczynski, M. Q. Zhao, A. T. C. Johnson, S. Guéron, C. Mattevi, A. Ouerghi, and H. Bouchiat, Spin-orbit interaction induced in graphene by transition metal dichalcogenides, Phys. Rev. B **99**, 245402 (2019).

[26] T. S. Ghiasi, J. Ingla-Aynés, A. A. Kaverzin, and B. J. van Wees, Large proximity-induced spin lifetime anisotropy in transition-metal dichalcogenide/graphene heterostructures, Nano Lett. **17**, 7528 (2017).

[27] J. C. Leutenantsmeyer, J. Ingla-Aynés, J. Fabian, and B. J. van Wees, Observation of Spin-Valley-Coupling-Induced Large Spin-Lifetime Anisotropy in Bilayer Graphene, Phys. Rev. Lett. **121**, 127702 (2018).

[28] L. A. Benítez, J. F. Sierra, W. S. Torres, A. Arrighi, F. Bonell, M. V. Costache, and S. O. Valenzuela, Strongly anisotropic spin relaxation in graphene-transition metal dichalcogenide heterostructures at room temperature, Nat. Phys. **14**, 303 (2018).

[29] J. Xu, T. Zhu, Y. K. Luo, Y.-M. Lu, and R. K. Kawakami, Strong and Tunable Spin-Lifetime Anisotropy in Dual-Gated Bilayer Graphene, Phys. Rev. Lett. **121**, 127703 (2018).

[30] C. K. Safeer, J. Ingla-Aynés, F. Herling, J. H. Garcia, M. Vila, N. Ontoso, M. R. Calvo, S. Roche, L. E. Hueso, and F. Casanova, Room-temperature spin Hall effect in graphene/MoS_2 van der Waals heterostructures, Nano Lett. **19**, 1074 (2019).

[31] F. Herling, C. K. Safeer, J. Ingla-Aynés, N. Ontoso, L. E. Hueso, and F. Casanova, Gate tunability of highly efficient spin-to-charge conversion by spin Hall effect in graphene proximitized with WSe_2, APL Mater. **8**, 071103 (2020).

[32] L. A. Benítez, W. Savero Torres, J. F. Sierra, M. Timmermans, J. H. Garcia, S. Roche, M. V. Costache, and S. O. Valenzuela, Tunable room-temperature spin galvanic and spin Hall effects in van der Waals heterostructures, Nat. Mater. **19**, 170 (2020).

[33] A. Md. Hoque, D. Khokhriakov, B. Karpiak, and S. P. Dash, Charge-spin conversion in layered semimetal $TaTe_2$ and spin injection in van der Waals heterostructures, Phys. Rev. Res. **2**, 033204 (2020).

[34] T. S. Ghiasi, A. A. Kaverzin, P. J. Blah, and B. J. van Wees, Charge-to-spin conversion by the Rashba-Edelstein effect in two-dimensional van der Waals heterostructures up to room temperature, Nano Lett. **19**, 5959 (2019).

[35] D. Khokhriakov, A. Md. Hoque, B. Karpiak, and S. P. Dash, Gate-tunable spin-galvanic effect in graphene-topological insulator van der Waals heterostructures at room temperature, Nat. Commun. **11**, 3657 (2020).

[36] L. Li, J. Zhang, G. Myeong, W. Shin, H. Lim, B. Kim, S. Kim, T. Jin, S. Cavill, B. S. Kim, C. Kim, J. Lischner, A. Ferreira, and S. Cho, Gate-tunable reversible Rashba-Edelstein effect in a few-layer graphene/2H-TaS_2 heterostructure at room temperature, ACS Nano **14**, 5251 (2020).

[37] M. Gmitra, D. Kochan, P. Högl, and J. Fabian, Trivial and inverted Dirac bands and the emergence of quantum spin Hall states in graphene on transition-metal dichalcogenides, Phys. Rev. B **93**, 155104 (2016).

[38] M. Milletari, M. Offidani, A. Ferreira, and R. Raimondi, Covariant Conservation Laws and the Spin Hall Effect in Dirac-Rashba Systems, Phys. Rev. Lett. **119**, 246801 (2017).

[39] A. W. Cummings, J. H. Garcia, J. Fabian, and S. Roche, Giant Spin Lifetime Anisotropy in Graphene Induced by Proximity Effects, Phys. Rev. Lett. **119**, 206601 (2017).

[40] J. H. Garcia, A. W. Cummings, and S. Roche, Spin Hall effect and weak antilocalization in graphene/transition metal dichalcogenide heterostructures, Nano Lett. **17**, 5078 (2017).

[41] M. Offidani, M. Milletari, R. Raimondi, and A. Ferreira, Optimal Charge-to-Spin Conversion in Graphene on Transition-

Metal Dichalcogenides, Phys. Rev. Lett. **119**, 196801 (2017).

[42] J. H. Garcia, M. Vila, A. W. Cummings, and S. Roche, Spin transport in graphene/transition metal dichalcogenide heterostructures, Chem. Soc. Rev. **47**, 3359 (2018).

[43] Y. S. Gani, E. J. Walter, and E. Rossi, Proximity-induced spin-orbit splitting in graphene nanoribbons on transition-metal dichalcogenides, Phys. Rev. B **101**, 195416 (2020).

[44] S. A. Cavill, C. Huang, M. Offidani, Y.-H. Lin, M. A. Cazalilla, and A. Ferreira, Proposal for Unambiguous Electrical Detection of Spin-Charge Conversion in Lateral Spin Valves, Phys. Rev. Lett. **124**, 236803 (2020).

[45] A. M. Alsharari, M. M. Asmar, and S. E. Ulloa, Topological phases and twisting of graphene on a dichalcogenide monolayer, Phys. Rev. B **98**, 195129 (2018).

[46] Y. Li and M. Koshino, Twist-angle dependence of the proximity spin-orbit coupling in graphene on transition-metal dichalcogenides, Phys. Rev. B **99**, 075438 (2019).

[47] A. David, P. Rakyta, A. Kormányos, and G. Burkard, Induced spin-orbit coupling in twisted graphene–transition metal dichalcogenide heterobilayers: Twistronics meets spintronics, Phys. Rev. B **100**, 085412 (2019).

[48] A. Pezo, Z. Zanolli, N. Wittemeier, P. Ordejón, A. Fazzio, S. Roche, and J. H. Garcia, Manipulation of spin transport in graphene/transition metal dichalcogenide heterobilayers upon twisting, 2D Mater. **9**, 015008 (2022).

[49] C. L. Kane and E. J. Mele, Quantum Spin Hall Effect in Graphene, Phys. Rev. Lett. **95**, 226801 (2005).

[50] H. Min, J. E. Hill, N. A. Sinitsyn, B. R. Sahu, L. Kleinman, and A. H. MacDonald, Intrinsic and Rashba spin-orbit interactions in graphene sheets, Phys. Rev. B **74**, 165310 (2006).

[51] S. Konschuh, M. Gmitra, and J. Fabian, Tight-binding theory of the spin-orbit coupling in graphene, Phys. Rev. B **82**, 245412 (2010).

[52] K. Zollner, A. W. Cummings, S. Roche, and J. Fabian, Graphene on two-dimensional hexagonal BN, AlN, and GaN: Electronic, spin-orbit, and spin relaxation properties, Phys. Rev. B **103**, 075129 (2021).

[53] X. Yang, B. Sa, P. Lin, C. Xu, Q. Zhu, H. Zhan, and Z. Sun, Tunable contacts in graphene/InSe van der Waals heterostructures, J. Phys. Chem. C **124**, 23699 (2020).

[54] K. Zollner, M. D. Petrović, K. Dolui, P. Plecháč, B. K. Nikolić, and J. Fabian, Scattering-induced and highly tunable by gate damping-like spin-orbit torque in graphene doubly proximitized by two-dimensional magnet $Cr_2Ge_2Te_6$ and monolayer WS_2, Phys. Rev. Res. **2**, 043057 (2020).

[55] K. Zollner and J. Fabian, Single and bilayer graphene on the topological insulator Bi_2Se_3: Electronic and spin-orbit properties from first principles, Phys. Rev. B **100**, 165141 (2019).

[56] K. Kandrai, P. Vancsó, G. Kukucska, J. Koltai, G. Baranka, Á. Hoffmann, Á. Pekker, K. Kamarás, Z. E. Horváth, A. Vymazalová, L. Tapasztó, and P. Nemes-Incze, Signature of large-gap quantum spin hall state in the layered mineral jacutingaite, Nano Lett. **20**, 5207 (2020).

[57] B. Fülöp, A. Márffy, S. Zihlmann, M. Gmitra, E. Tóvári, B. Szentpéteri, M. Kedves, K. Watanabe, T. Taniguchi, J. Fabian, C. Schönenberger, P. Makk, and S. Csonka, Boosting proximity spin–orbit coupling in graphene/WSe_2 heterostructures via hydrostatic pressure, npj 2D Mater. Appl. **5**, 82 (2021).

[58] See Supplemental Material at http://link.aps.org/supplemental/10.1103/PhysRevResearch.4.L022049 for (i) discussion of the symmetry properties of the quantum phase ϑ_R, (ii) details of the numerical calculations shown in Figs. 1–2, (iii) brief discussion of supermoire effects, (iv) details of the magnetotransport calculations shown in Fig. 3, (v) brief discussion of another setup to investigate twist angle dependent transport in a graphene-TMDC heterostructure.

[59] S. Fang, R. Kuate Defo, S. N. Shirodkar, S. Lieu, G. A. Tritsaris, and E. Kaxiras, *Ab initio* tight-binding Hamiltonian for transition metal dichalcogenides, Phys. Rev. B **92**, 205108 (2015).

[60] D. Pierucci, H. Henck, J. Avila, A. Balan, C. H. Naylor, G. Patriarche, Y. J. Dappe, M. G. Silly, F. Sirotti, A. T. C. Johnson, M. C. Asensio, and A. Ouerghi, Band alignment and minigaps in monolayer MoS_2-graphene van der Waals heterostructures, Nano Lett. **16**, 4054 (2016).

[61] H. Nakamura, A. Mohammed, Ph. Rosenzweig, K. Matsuda, K. Nowakowski, K. Küster, P. Wochner, S. Ibrahimkutty, U. Wedig, H. Hussain, J. Rawle, C. Nicklin, B. Stuhlhofer, G. Cristiani, G. Logvenov, H. Takagi, and U. Starke, Spin splitting and strain in epitaxial monolayer WSe_2 on graphene, Phys. Rev. B **101**, 165103 (2020).

[62] T. Naimer, K. Zollner, M. Gmitra, and J. Fabian, Twist-angle dependent proximity induced spin-orbit coupling in graphene/transition metal dichalcogenide heterostructures, Phys. Rev. B **104**, 195156 (2021).

[63] We describe the energy of the Dirac point of graphene in the band gap of the TMDC by a number $f_G \in [0, 1]$. Its value is a linear function of the position of the Dirac point in the TMDC band gap. When $f_G = 0$, the Dirac point is aligned with the TMDC valence band edge, for $f_G = 1$ the Dirac point has the same energy as the TMDC conduction band edge. In the calculations involving MoS_2, we used DFT parameters $E_g = 1.807$ eV, $f_G = 0.974$ and experimental parameters [60] $E_g = 2$ eV, $f_G = 0.55$. In the case of WSe_2, DFT parameters were $E_g = 1.638$ eV, $f_G = 0.161$ and experimental ones [61] $E_g = 1.95$ eV, $f_G = 0.426$.

[64] M. Andjelković, S. P. Milovanović, L. Covaci, and F. M. Peeters, Double moiré with a twist: Supermoiré in encapsulated graphene, Nano Lett. **20**, 979 (2020).

[65] H. Oka and M. Koshino, Fractal energy gaps and topological invariants in hBN/graphene/hBN double moiré systems, Phys. Rev. B **104**, 035306 (2021).

[66] M. Offidani and A. Ferreira, Microscopic theory of spin relaxation anisotropy in graphene with proximity-induced spin-orbit coupling, Phys. Rev. B **98**, 245408 (2018).

[67] A. F. Young and P. Kim, Quantum interference and Klein tunnelling in graphene heterojunctions, Nat. Phys. **5**, 222 (2009).

[68] P. Rickhaus, R. Maurand, M.-H. Liu, M. Weiss, K. Richter, and C. Schönenberger, Ballistic interferences in suspended graphene, Nat. Commun. **4**, 2342 (2013).

[69] P. Rickhaus, P. Makk, M.-H. Liu, E. Tóvári, M. Weiss, R. Maurand, K. Richter, and C. Schönenberger, Snake trajectories in ultraclean graphene p–n junctions, Nat. Commun. **6**, 6470 (2015).

[70] S. Chen, Z. Han, M. M. Elahi, K. M. Masum Habib, L. Wang, B. Wen, Y. Gao, T. Taniguchi, K. Watanabe, J. Hone, A. W. Ghosh, and C. R. Dean, Electron optics with p-n junctions in ballistic graphene, Science **353**, 1522 (2016).

[71] C. Handschin, P. Makk, P. Rickhaus, M.-H. Liu, K. Watanabe, T. Taniguchi, K. Richter, and C. Schönenberger, Fabry-Perot resonances in a graphene/hBN moiré superlattice, Nano Lett. **17**, 328 (2017).

[72] A. V. Shytov, M. S. Rudner, and L. S. Levitov, Klein Backscattering and Fabry-Pérot Interference in Graphene Heterojunctions, Phys. Rev. Lett. **101**, 156804 (2008).

[73] A. Silva, V. E. P. Claerbout, T. Polcar, D. Kramer, and P. Nicolini, Exploring the stability of twisted van der Waals heterostructures, ACS Appl. Mater. Interfaces **12**, 45214 (2020).